Routes to identification of intrinsic twist in helical MoS_{2} nanotubes by electron diffraction and annular dark-field scanning transmission electron microscopy imaging

A. Mittal, D.-B. Zhang, C. Teresi, T. Dumitrică, and K. A. Mkhoyan

Phys. Rev. B **84**, 153401 — Published 4 October 2011

DOI: 10.1103/PhysRevB.84.153401

Routes to identification of intrinsic twist in helical MoS_2 nanotubes by electron diffraction and annular dark field-scanning transmission electron microscopy imaging

A. Mittal[1], D.-B. Zhang[2], C. Teresi[1,3], T. Dumitrică[2]*, and, K.A. Mkhoyan[1]*
[1] *Department of Chemical Engineering and Materials Science, University of Minnesota, Minneapolis, Minnesota 55455*
[2] *Department of Mechanical Engineering, University of Minnesota, Minneapolis, MN 55455*
[3] *School of Materials Science and Engineering, Clemson University, Clemson, SC 29634*
(Dated: September 19, 2011)

Objective molecular dynamics simulations coupled with a density functional-based tight-binding model indicated that a stress-free single-walled $(14, 6)$ MoS_2 nanotube exhibits a torsional deformation of 0.87 deg/nm. Simulated electron diffraction patterns and atomic-resolution annular dark field scanning transmission electron microscopy (ADF-STEM) images of the computed nanotube structures show promise that this peculiar feature can be identified experimentally. The small intrinsic twist removes the translational periodicity prescribed by the rolled-up construction and defines a nanotube for which the atomic order is most fundamentally described by the objective structures concept.

PACS numbers: 61.46.-w, 61.46.Fg, 61.48.De

One of the most promising families of nansocale materials is single walled nanotubes (NTs). While identification of chirality in NTs with atomically-thin walls such as C NTs[2] and BN NTs[3,4] has been pursued[5,6], little is known about other helical NTs with more complex walls, such as MoS_2, WS_2, and TiS_2[7–12]. These inorganic NTs have already found many applications, especially related to their mechanical properties[13] and their ability to store hydrogen[14]. Identification of the equilibrium atomic structure of NTs plays a key role in understanding their structure-property relationships, and therefore detailed characterization of their natural atomic structures is essential.

The atomic structure of NTs is usually conceptualized by rolling up a flat ribbon into a seamless cylinder. The chiral NT indices (n, m) are used to describe the angle of rolling[15]. In this rolling process, associated with pure linear elastic mechanical bending, the circumference vector becomes a circle, while the translation vector stays straight. The expectation is that during the structural optimization, the translational symmetry is preserved. Thus, microscopic treatments formulated under periodic boundary conditions are applied to determine the optimal translational periodicity and the location of atoms in one translational cell. Although not widely used, quantum treatments that make use of helical instead of the translational symmetry are also available[16,17]. Using objective molecular dynamics[16] (MD) coupled with symmetry-adapted nonorthogonal tight-binding[17] implemented in Trocadero[18] and a density functional-based tight binding (DFTB) model[19,20], we have previously confirmed[21] that the rolled-up predictions are also valid in large diameter chiral MoS_2 NTs. However, under ~ 7 nm in diameter, the rolled-up construction was increasingly inaccurate especially for near 15 degrees chiral NTs. The rolling-up process becomes nonlinear elastic and the translation vector turns into a helix instead of staying straight. We refer to these structures as NTs with intrinsic twist.

Recently, a variety of structures such as C NTs, viral capsids, and many proteins, have been categorized by using the concept of objective structures[22]. The surprising intrinsic twist result has fundamental implications since it predicts the existence of NTs for which the atomic order is most fundamentally described as an objective structure[22] rather than a crystalline one. In this work we actualize these predictions with simulations showing that a careful analysis of the electron diffraction pattern (EDP) obtained from a twisted MoS_2 NT using transmission electron microscope (TEM) can be a route for proving the existence of the peculiar intrinsic twist effect. Alternatively, if aberration-corrected scanning TEM (STEM) is available, analysis of the annular dark field (ADF) STEM images can be utilized as well.

Objective DFTB simulations with valence shell basis set comprised of *sp* and *spd* functions for the S and Mo atoms, respectively, were performed to obtain the zero-temperature atomic coordinates of MoS_2 NTs with and without intrinsic twist. The current study is focused on a $(14, 6)$ MoS_2 NT as its small diameter and nearness to a 15 degrees chirality make it more susceptible to the intrinsic twisting instability[21]. Based on the previous structural findings[21], here we carried out microscopic relaxation calculations of this NT described in the "angular-helical" representation[23–25] from a fundamental objective domain containing one molecule composed of only one Mo and two S atoms. The rolled-up NT is described with[16,22,24]

$$\mathbf{X}_{j,\zeta_1,\zeta_2} = \mathbf{R}_2^{\zeta_2}\,\mathbf{R}_1^{\zeta_1}\mathbf{X}_j + \zeta_1\mathbf{T}_1, \quad j = 1, 2, 3. \tag{1}$$

The rotational matrix $\mathbf{R}_2$ indicates an angular rotation of angle θ_2. The rotational matrix $\mathbf{R}_1$ (of angle θ_1) and the axial vector $\mathbf{T_1}$ indicate a helical operation. These angular and helical operations have a common axis. Index j runs over the three atoms (the molecule) at locations $\mathbf{X}_j$ inside the fundamental objective domain. Integers ζ_1 and ζ_2, with $-\infty < \zeta_1 < \infty$ and $\zeta_2 = 0, 1$, label the various replicas of the initial three-atom domain. Ideal values for $\theta_2 = 180$ deg and $\theta_1 = 53.54$ deg corresponding to the rolled-up construction can be obtained, for example by following the approach[23] summarized in Ref. 24. First, the NT structure was optimized to identify the optimal $|\mathbf{T_1}|$ value. By keeping θ_1 and θ_2 at their rolled-up predictions, we ensure that the predicted translational periodicity is maintained. 1,000 uniformly distributed helical k-points and 2 angular numbers were used to converge the band energy. Next, we varied θ_1 to $\theta_1 + \gamma|\mathbf{T_1}|$ in order to determine whether the axial relaxation is sufficient to optimize the structure.

The results presented in Fig. 1 demonstrate that when the twist rate γ is varied, the stable minimum of the structure does not correspond to $\gamma = 0$ deg/nm. Variations in θ_1 lower the energy of the structure, which finally achieves a stress-free state with a residual twist of 0.87 deg/nm. This is in agreement with our previous objective MD simulations carried out on a larger objective domain.

Two existing TEM techniques can be employed to observe the intrinsic twist in MoS_2 NTs: electron diffraction and atomic-resolution imaging. Other techniques that are used to identify the (n, m) indices of NTs, such as Raman spectroscopy[28] and scanning tunnelling microscopy (STM)[5], appear to be at a disadvantage. The intrinsic twist does not change the (n, m) indices and the applicability of Raman spectroscopy to identify small torsional deformation is untested. The wall of a MoS_2 NT is actually a complex 3-atomic-layer system, Fig. 1(a), and the use of STM for structural characterization becomes less reliable.

Electron diffraction has previously been used for characterization of NTs[2,29] and especially for structural features caused by different chiral arrangements[19,30]. For instance, the existence of armchair and zigzag MoS_2 NTs was confirmed by comparing experimental EDPs with simulated ones[19]. Chiral indices of a variety of C NTs have been determined by electron diffraction analysis[5,31,32]. The chirality of various NTs, including Au and Ag-alloyed MoS_2 and WS_2, has also been studied by electron diffraction[8].

To determine if there are substantial differences between the EDPs of MoS_2 NTs with and without twist, here we simulated EDPs of both types of NTs using the *Multislice* programs developed by Kirkland[33] based on the algorithm introduced by Cowley and Moodie[34]. Models of 20 nm long (14,6) MoS_2 NTs were constructed using atomic coordinate files obtained via microscopic calculations discussed earlier. A grid of 2048 x 2048 pixels with reciprocal pixel size 0.045 nm^{-1} was used in these simulations. A 100 keV electron beam incident normal to the NT axis was used as this is the most common orientation of NTs in an experimental set-up. Propagation of the electron beam through the entire specimen was achieved by passing the beam through 1 Å slices. The effect of temperature was modeled by averaging 20 frozen phonon configurations at 298 K. Root-mean-square displacements of 0.071 Å and 0.045 Å were used for S and Mo atoms respectively, which were obtained from corresponding Debye-Waller factors for similar MoS_2 compounds[35]. Non-physical high frequency artifacts were filtered out by convoluting the EDPs with a Gaussian function of standard deviation 0.045 nm^{-1}.

EDPs of (14,6) MoS_2 NTs with and without twist are shown in logarithmic scale in Fig. 2(a) and (b). The diffraction spots are elongated due to the cylindrical structure of the NT[30]. EDPs from NTs show *mm2* symmetry in (*hk0*) spots[2]. As only (*hk0*) spots are present in EDP of a single wall NT, the analysis of one quadrant of the EDP is sufficient for identifying differences. To characterize the differences between diffraction spots, the distance between the equatorial line and each diffraction spot was measured, as shown in Fig. 2 (a), and the results are tabulated in Table I. The error in the position of the diffraction spot was estimated by measuring the variation in the position of peak intensity of the diffraction spot at different locations along the elongated spot. A maximum variation of ± 0.05 nm^{-1} was observed. The range of diffraction spot position among the 20 frozen phonon configurations was less than 0.0018 nm^{-1}, which is significantly lower than the sampling error. The largest difference in the positions of diffraction spots obtained from (14,6) MoS_2 NT with and without twist was 0.09 nm^{-1} and that was observed for spots D_3 and A_1. The difference is clearly above the error level and, therefore, can be used to identify presence of the intrinsic twist.

Additional EDPs of (14±1,6±1) MoS_2 NTs, i.e. (15,6), (13,6), (14,5), and (14,7) NTs, were simulated, Fig. 2(c-f), in order to ensure that the above differences in EDPs due to presence of an intrinsic twist can be distinguished from those due to small changes in chiral indices. The intrinsic twist was not considered in these additional NTs. As can be observed in Table 1, the differences between D_i ($i = 1, 2, 3$) and A_1 values for (14,6) and other chiral NTs are considerably larger than between those from (14,6) NTs with and without intrinsic twist. Thus, the intrinsic twist cannot be confused with other chiral NTs.

Atomic resolution ADF-STEM images can be alternatively used to detect the intrinsic twist. Unlike conventional bright field TEM imaging, ADF-STEM imaging avoids complications in image interpretation due to focusing conditions. Here ADF-STEM image intensity is directly dependent on atomic number of scattering atom[36,37]. Simulations of ADF-STEM images were carried out using using the same *Multislice* code used above to simulate EDPs. The probe parameters used in simulations were: 100 keV incident beam energy, $C_{s(3)}$=-0.015 mm and $C_{s(5)}$=10 mm for spherical

aberration coefficients, Δf=$-$30 Å for defocus, and α_{obj}=25 mrad for objective aperture, which provide a converged probe with a FWHM of 0.8 Å[38,39]. The images were calculated with a 7.4 pixels/Å sampling.

Simulated atomic resolution ADF-STEM images of characteristic sections of (14,6) MoS_2 NTs with and without intrinsic twist are shown in Figs. 3 (a) and (b). The projected positions of the Mo and S atoms in most cases can be identified: Mo atoms as bigger and brighter spots and S atoms as smaller and dimmer spots. In an actual experiment the exact orientation of the suspended NT relative to the incident beam is difficult to control. Therefore, to understand the effects on images of NT rotation relative to its axis, we also simulated ADF-STEM images of the same NTs after rotating both of them by 15 degrees. The resulting images are presented in Fig. 3 (c) and (d), respectively. As can be seen, the rotation along the tube axis is equivalent to a shift in the imaging area. Specifically, a 15 degrees rotation corresponds to a 2.1 Å shift.

The simulated ADF-STEM image of a (14,6) MoS_2 NT without intrinsic twist has two bright spots in the middle of the NT, highlighted by dotted circles, while the ADF-STEM image of (14,6) MoS_2 NT with intrinsic twist is missing a bright spot in one of these locations, compare Fig. 3 (c) and (d). Comparison with atomic models shows that the bright spot in the larger circle corresponds to the projected image of two Mo atoms and the bright spot in the smaller circle corresponds to the projected image of four sulfur atoms. Such distinctive features provide an alternate route for identifying the intrinsic twist.

In conclusion, our presented simulations show that in spite of the small diameter and the complexity of the MoS_2 wall, the atomic-scale intrinsic twist in a MoS_2 NT predicted by simulations could be observed in experiment by either electron diffraction using conventional TEM or atomic-resolution ADF-STEM imaging using aberration-corrected STEM. We envision that these techniques can be utilized in other small diameter chiral NTs predicted to exhibit intrinsic twists of similar magnitude, such as C NTs[25,26], BN NTs[26], and TiS_2 NTs[27].

We thank G. Seifert for providing the MoS_2 DFTB parameters. This work was partially supported by the NSF MRSEC program DMR-0819885 and the Abu Dhabi-Minnesota Institute for Research Excellence (ADMIRE), a partnership between the Petroleum Institute of Abu Dhabi and the Department of Chemical Engineering and Materials Science of the University of Minnesota. D.-B.Z and T.D. thank NSF CAREER Grant CMMI-0747684 and AFOSR Grant FA9550-09-1-0339. Computational resources from the University of Minnesota Supercomputing Institute were used.

[*] Corresponding authors: td@me.umn.edu (TD) and mkhoyan@umn.edu (KAM).
[2] S. Iijima, *Nature* **354**, 56 (1991).
[3] N.G. Chopra, R.J. Luyken, K. Cherrey, V.H. Crespi, M.L. Cohen, S.G. Louie, and A. Zettl, *Science* **269**, 966 (1995).
[4] D. Golberg, Y. Bando, Y. Huang, T. Terao, M. Mitome, C. C. Tang, and C. Y. Zhi, *ACS Nano* **4**, 2979 (2010).
[5] A. Jurio, M. Dresselhaus, and G. Dresselhaus, *Carbon Nanotubes*, Springer (2008).
[6] H. Lin, J. Lagoute, V. Repain, C. Chacon, Y. Girard, F. Ducastelle, H. Amara, A. Loiseau, P. Hermet, L. Henrard, and S. Rousset, *Phys. Rev. B* **81**, 235412 (2010).
[7] P. Santiago, J.A. Ascencio, D. Mendoza, M. Perez-Alvarez, A. Espinosa, C. Reza-SanGermaan, P. Schabes-Retchkiman, G.A. Camacho-Bragado, and M. Jose-Yacamaan, *Appl. Phys. A.* **78**, 513 (2004).
[8] M. Remskar, Z. Skraba, P. Stadelmann, and F. Levy, *Adv. Mat.* **12**, 814 (2000).
[9] M. Remskar, A. Mrzel, Z. Skraba, A. Jseih, M. Ceh, J. Demsar, P. Stadelmann, F. Levy, and D. Mihailovic, *Science* **292**, 479 (2001).
[10] Y. Feldman, E. Wasserman, D.J. Srolovitz, and R. Tenne, *Science* **267**, 222 (1995).
[11] K.S. Coleman, J. Sloan, N.A Hanson, G. Brown, G. P. Clancy, M. Terrones, H. Terrones, and M. L. H. Green, *J. Am. Chem. Soc.* **124**, 11580 (2002).
[12] J. Chen, Z.-L. Tao, S.-L. Li, X.-B. Fan, and S.-L. Chou, *Adv. Mater.* **15**, 1379 (2003).
[13] R. Tenne and C.N.R. Rao, *Philos. Trans. R. Soc. A* **362**, 2099 (2004).
[14] J. Chen, S.-L. Li, Z.-L. Tao, Y.-T. Shen, and C.-X. Cui, *J. Am. Chem. Soc.* **125**, 5284 (2003).
[15] R. Saito, G. Dresselhaus, and M.S. Dresselhaus, *Physical Properties of Carbon Nanotubes*, Imperial College Press, London, UK (1998).
[16] T. Dumitrică and R.D. James, *J. Mech. Phys. Solids* **55**, 2206 (2007).
[17] D.-B. Zhang, M. Hua, and T. Dumitrică, *J. Chem. Phys.* **128**, 084104 (2008).
[18] R. Rurali and E. Hernandez, *Comp. Mat. Sci.* **28**, 85 (2003).
[19] G. Seifert, H. Terrones, M. Terrones, G. Jungnickel, and Th. Frauenheim, *Phys. Rev. Lett.* **85**, 146 (2000).
[20] I. Milosevic, B. Nikolic, E. Dobardzic, M. Damnjanovic, I. Popov, and G. Seifert, *Phys. Rev. B* **76**, 233414 (2007).
[21] D.-B. Zhang, T. Dumitrică, and G. Seifert, *Phys. Rev. Lett.* **104**, 065502, (2010).
[22] R.D. James, *J. Mech. Phys. Solids* **54**, 2354 (2006).
[23] Ge. G. Samsonidze, R. Saito, A. Jorio, M. A. Pimenta, A. G. Souza Filho, A. Gruneis, G. Dresselhaus, and M. S. Dresselhaus, *J. Nanosci. Nanotech.* **3**, 431 (2003); E.B. Barros, A. Jorio, Ge.G. Samsonidze, R.B. Capaz, A.G. Souza Filho, J. Mendes Filho, G. Dresselhaus, and M.S. Dresselhaus, *Phys. Rep.* **431**, 261 (2006).
[24] D.-B. Zhang and T. Dumitrică, *Appl. Phys. Lett.* **93**, 031919 (2008).
[25] D.G. Vercosa, E.B. Barros, A.G.S. Filho, J. M. Filho, Ge.G. Samsonidze, R. Saito, and M.S. Dresselhaus, *Phys. Rev. B* **81**, 165430 (2010).
[26] D.-B. Zhang, E. Akatyeva, and T. Dumitrică *Phys. Rev. B* (at press).
[27] D. Teich, T. Lorenz, J.-O. Joswig, G. Seifert, D.-B. Zhang, and T. Dumitrică, *J. Phys. Chem. C* **115**, 6392 (2011).
[28] N. Anderson, A. Hartschuh, and L. Novotny, *Nano Lett.* **7**, 577 (2007).
[29] R. Tenne, L. Margulis, M. Genut, and G. Hodes, *Nature* **360**, 444 (1992).
[30] J.C. Meyer, M. Paillet, G.S. Duesberg and S. Roth, *Ultramicroscopy* **106**, 176 (2006).
[31] Z. Liu and L. Qin, *Chem. Phys. Lett.* **408**, 75 (2005).
[32] H. Deniz, A. Derbakova, and L.-C. Qin, *Ultramicroscopy* **111**, 66, (2010).
[33] E.J. Kirkland, *Advanced Computing in Electron Microscopy*, 2nd edition Springer, (2010).
[34] J.M. Cowley and A.F. Moodie, *Acta. Cryst.* **10**, 609 (1957).
[35] P. Afanasiev and I. Bezverkhy, *Chem. Mater.* **14**, 2826 (2002).
[36] E.J. Kirkland, R.F. Loane, and J. Silcox, *Ultramicroscopy* **23**, 77 (1987).
[37] S.J. Pennycook and L.A. Boatner, *Nature* **336**, 565 (1988); S.J. Pennycook, *Ultramicroscopy* **30**, 58 (1989).
[38] K.A. Mkhoyan, P.E Batson, J. Cha, W.J. Schaff and J. Silcox, *Science* **312**, 1354 (2006).
[39] K.A. Mkhoyan, S.E. Maccagnano-Zacher, E.J. Kirkland, and J. Silcox, *Ultramicroscopy* **108**, 791 (2008).

TABLE I: Distances between diffraction spots and equatorial line for different NTs.

NT	Distance from equatorial line (nm^{-1}) ± 0.05 nm^{-1}			
	D_1	D_2	D_3	A_1
(14,6) Twisted	3.33	2.57	0.77	1.71
(14,6)	3.38	2.57	0.86	1.80
(14,5)	3.65	2.61	1.04	2.07
(15,6)	3.65	2.66	0.95	1.71
(14,7)	3.33	2.61	0.72	1.89
(13,6)	3.60	2.75	0.86	1.89

FIG. 1: (a) A stress-free (14,6) MoS_2 NT. Light gray are S and gray are Mo. (b) Strain energy as a function of twist rate. The arrow point to the energy minimum corresponding to the stress-free structure with intrinsic twist.

FIG. 2: EDPs of different MoS_2 NTs: (a) (14,6), (b) (14,6) NT with intrinsic twist, (c) (14,5), (d) (15,6), (e) (14,7) and, (f) (13,6). EDPs are shown in logarithmic scale.

FIG. 3: ADF-STEM images of MoS_2 (14,6) NT (a) without and (b) with intrinsic twist. (c) and (d) ADF-STEM images of the same tubes as in (a) and (b), respectively, after rotating NTs by 15° along the tube axis.

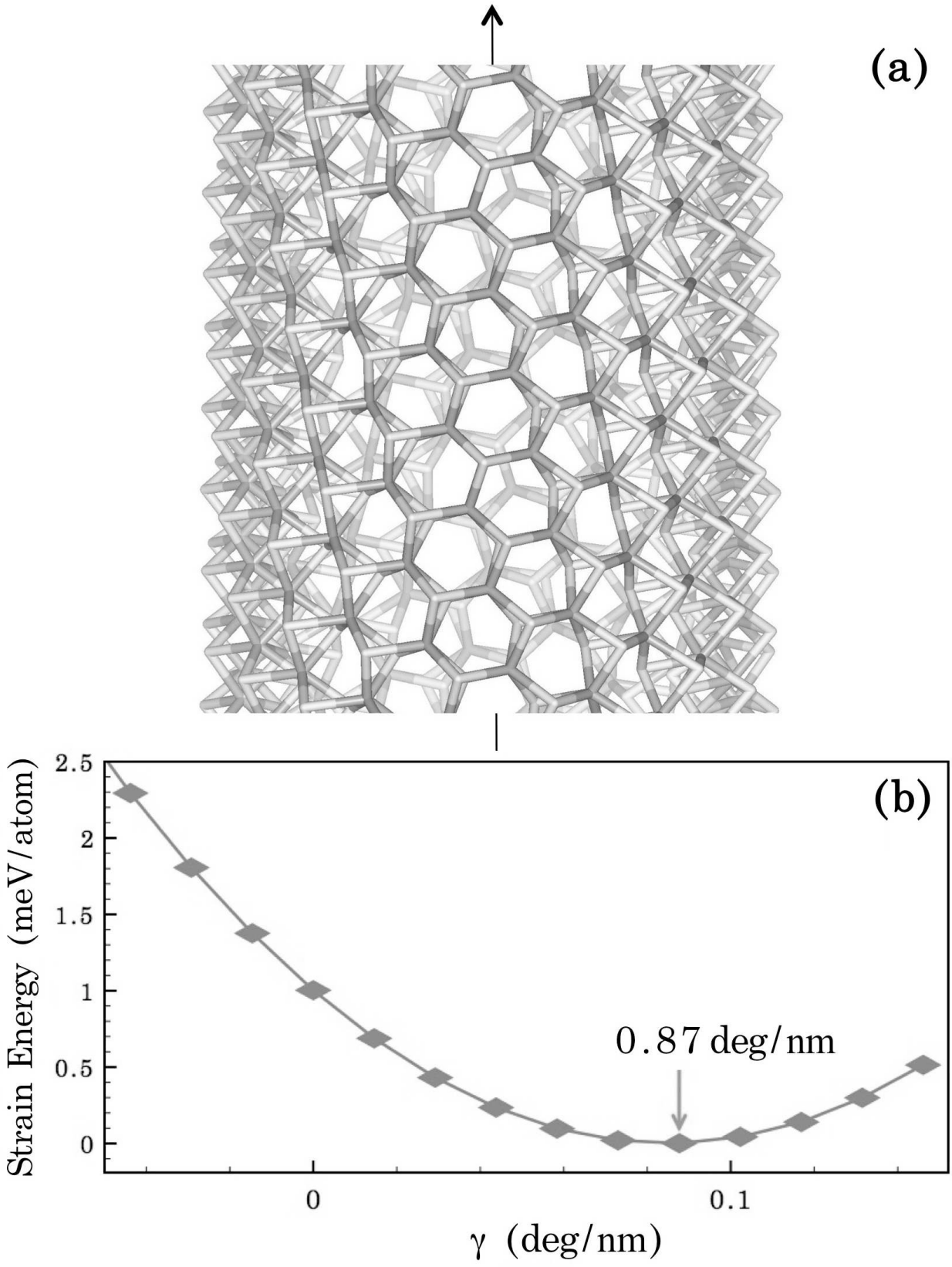

Figure 1 BGR1240 19Sep2011

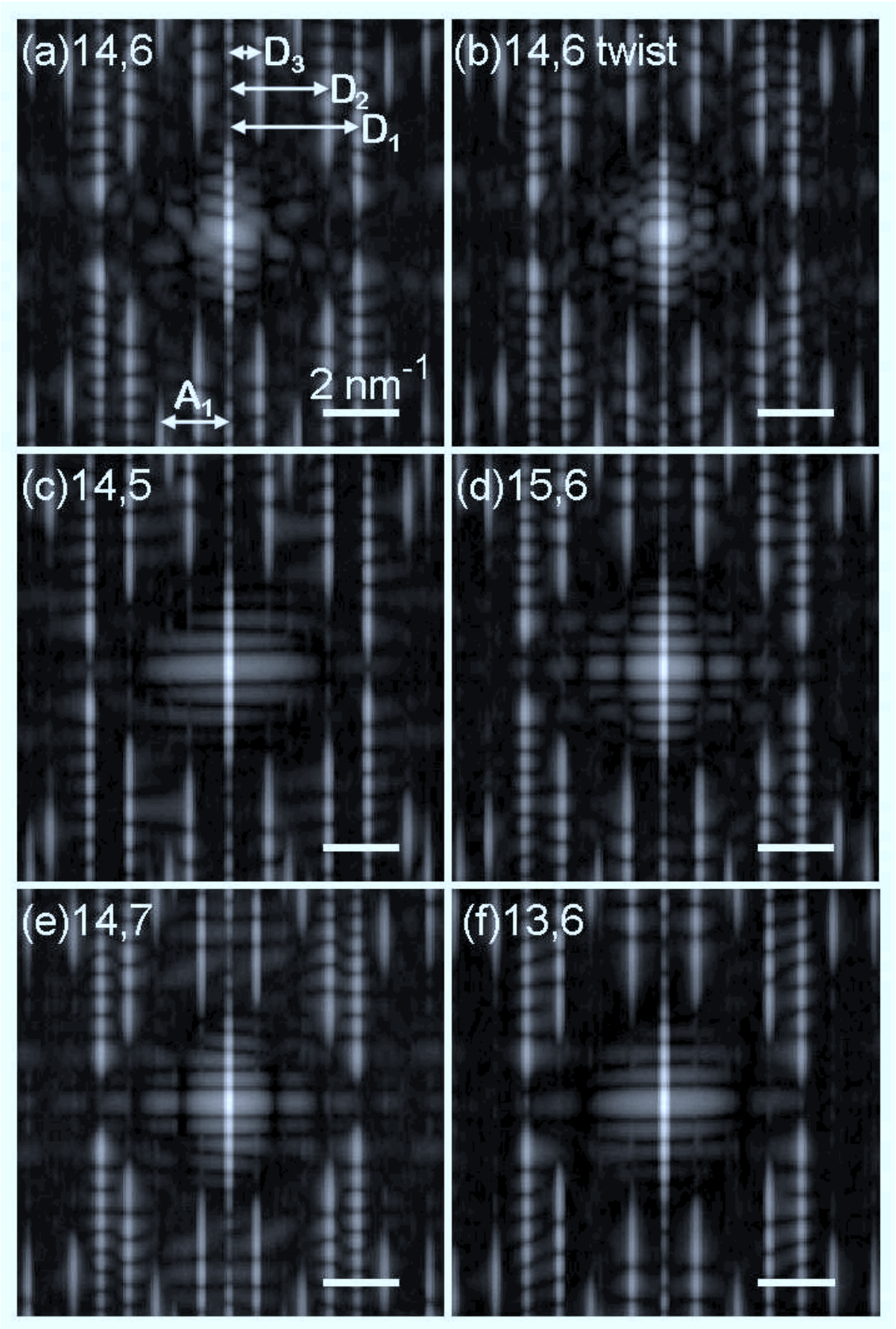

Figure 2 BGR1240 19Sep2011

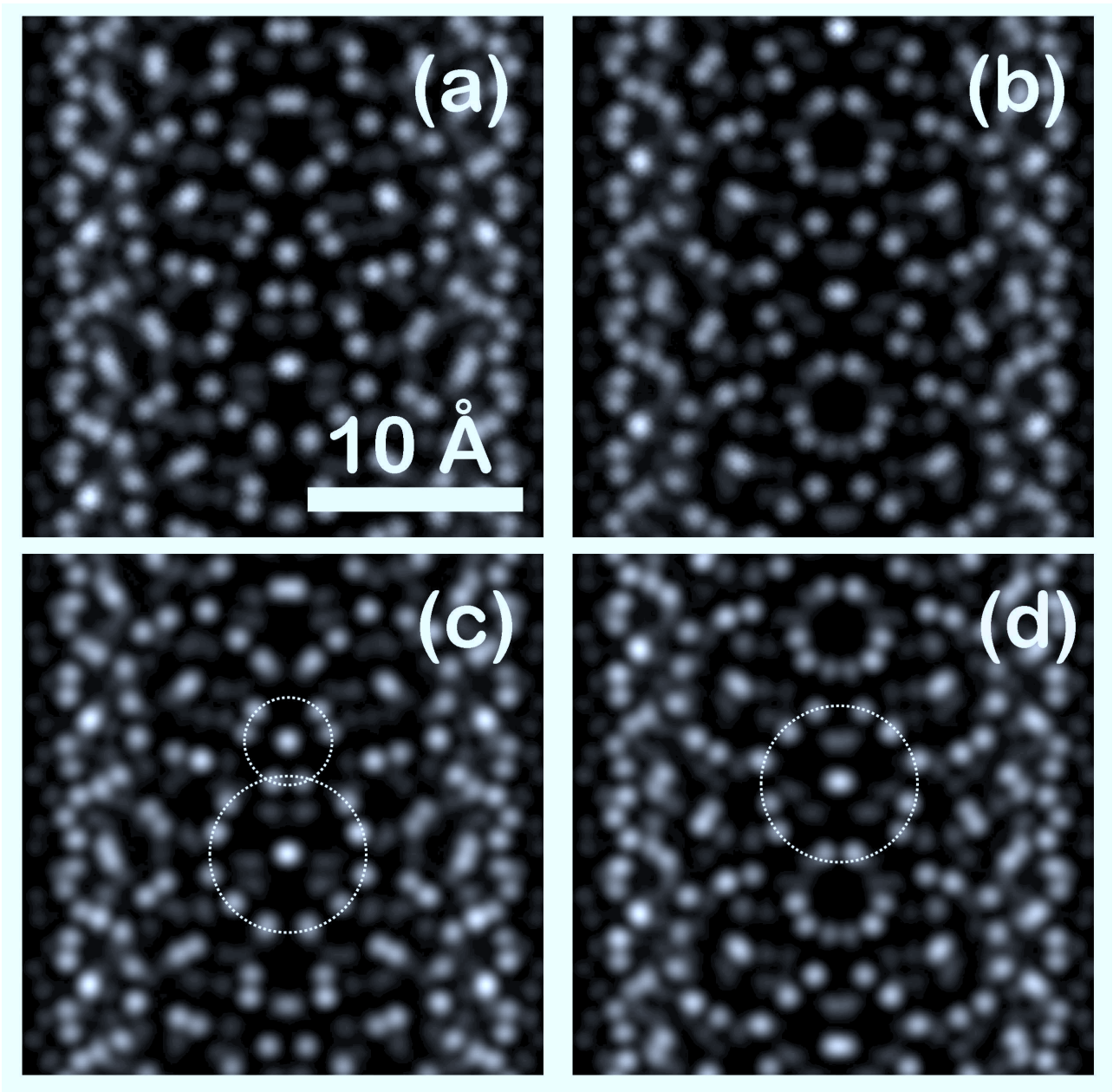

Figure 3 BGR1240 19Sep2011